

Nanoscale

Accepted Manuscript

This article can be cited before page numbers have been issued, to do this please use: X. Zhu, D. T. N. Tram, D. M. Murali, V. A. Barathi, V. Mayandi, R. Lakshminarayanan and P. L. R. Ee, *Nanoscale*, 2025, DOI: 10.1039/D5NR01674F.



This is an Accepted Manuscript, which has been through the Royal Society of Chemistry peer review process and has been accepted for publication.

Accepted Manuscripts are published online shortly after acceptance, before technical editing, formatting and proof reading. Using this free service, authors can make their results available to the community, in citable form, before we publish the edited article. We will replace this Accepted Manuscript with the edited and formatted Advance Article as soon as it is available.

You can find more information about Accepted Manuscripts in the [Information for Authors](#).

Please note that technical editing may introduce minor changes to the text and/or graphics, which may alter content. The journal's standard [Terms & Conditions](#) and the [Ethical guidelines](#) still apply. In no event shall the Royal Society of Chemistry be held responsible for any errors or omissions in this Accepted Manuscript or any consequences arising from the use of any information it contains.

ARTICLE

Antimicrobial Peptide-Conjugated Graphene Coatings for Prevention and Treatment of Bacterial Infections

Xiao Zhu,^a Nhan Dai Thien Tram,^a Dhanya Mahalakshmi Murali,^a Veluchamy Amutha Barathi,^b Mayandi Venkatesh,^b Rajamani Lakshminarayanan,^{a,b} and Pui Lai Rachel Ee^{*a}

Received 00th January 20xx,
Accepted 00th January 20xx

DOI: 10.1039/x0xx00000x

Graphene, a two-dimensional hexagonal lattice of carbon atoms, displays remarkable physicochemical properties. In contrast to classical chemical exfoliation, chemical vapour deposition (CVD) technology has enabled the production of continuous transparent graphene. CVD graphene coatings on biomedical devices such as contact lenses (CLs) offer several advantages, such as shielding from electromagnetic wave interference and dehydration protection. However, its protective effect against bacteria adhesion remains unexplored. In this study, we designed a series of antimicrobial peptide (AMP)-modified CVD graphene coating on polydimethylsiloxane (PDMS), a biocompatible CLs material. AMPs were successfully conjugated on CVD graphene coating, with negligible impact on the light transmittance. The resultant coating displayed contact angles of less than 50° and protein deposition of less than 9.4 μg cm⁻², indicating transparency, wettability, and protein deposition suitable for biomedical devices. AMPs conjugation on the graphene surface prevented biofilm formation by *Pseudomonas aeruginosa* (*P. aeruginosa*), as evidenced by lower colony counts and bacterial metabolic activity. The antimicrobial activity and biocompatibility of the coatings were further demonstrated using *ex vivo* porcine skins and *in vivo* rabbit eyes respectively. Overall, this study highlights the potential of AMP-modified CVD graphene coating to minimize bacterial infection and prevent biofilm formation.

Introduction

Bacterial infections associated with the use of biomedical devices pose serious healthcare threats¹. With long-term usage, bacteria gradually attach to the device surface and develop biofilms, which render the pathogens less susceptible to antimicrobial killing^{2–6}. Antibiotic flushes or device replacements are not efficient at eliminating the resulting infections. Biofilm formation is a dynamic process involving both planktonic bacteria and the solid surface⁷. Researchers have explored applying antimicrobial coatings to biomedical devices to reduce microbial adhesion and kill planktonic cells⁸. By virtue of extraordinary mechanical, electrical, chemical, and biocompatibility properties, graphene has been explored in a range of biomedical applications⁹. In antimicrobial applications^{10,11}, most studies focused on suspension systems using graphene oxide (GO) and reduced graphene oxide (rGO) synthesized via chemical exfoliation^{12–15}. Apart from exfoliation methods, chemical vapor deposition (CVD) technology has recently attracted attention in enabling highly controlled production of graphene with desirable properties including a flawless crystal structure, continuous large area, uniformity, transparency, and controllable layer number^{16–19}. The adhesion

between CVD graphene and polymeric substrates was shown to be durable enough to withstand physical changes during sterilization processes²⁰, thus rendering it suitable as coatings on biomedical devices. Polydimethylsiloxane (PDMS) is a biocompatible material widely used for constructing biomedical devices such as contact lenses (CLs), intraocular lenses, dressings, bandages, catheters, dental and bone implants²¹. However, PDMS is intrinsically incapable of resisting bacterial adhesion over long-term use, which we seek to address with our coating design.

In this work, we first explored the effect of CVD graphene coating on PDMS (G-PDMS). Using colony count and confocal microscopy, the anti-fouling activity of G-PDMS was shown to be better than uncoated PDMS against a range of pathogens, including in the presence of serum proteins to simulate body fluid. Apart from negligible cytotoxicity, human umbilical vein endothelial cells (HUVEC) grown on G-PDMS surface could differentiate into tube-like structures, which underlies the angiogenesis cascade. Building on these positive findings, we next synthesized a series of antimicrobial peptide (AMP)-modified CVD graphene through covalent conjugation. Three beta-hairpin peptides from our group's published work were selected as they displayed selective activity against clinically relevant gram-negative and we would like to further explore their possibility in antimicrobial use²². We also selected a broad-spectrum natural peptide Magainin 1, which can permeabilize bacteria membrane to kill pathogens. We would like to know if the peptides with different physical properties and antimicrobial activity profile will affect the conjugation process

^aDepartment of Pharmacy and Pharmaceutical Sciences, National University of Singapore, 117543, Singapore.

^bOcular Infections and Anti-microbials Research Group, Singapore Eye Research Institute, The Academia, 20 College Road, Discovery Tower, Singapore 169856, Singapore.
Supplementary Information available at DOI: 10.1039/x0xx00000x



and if the conjugation on the surface will affect antimicrobial activity of AMP. The success of peptide modification was validated using Fourier transform infrared (FTIR) spectra and X-ray photoelectron spectroscopy (XPS). The amount of conjugated peptides was quantified using the CBQCA (3-(4-carboxybenzoyl)quinoline-2-carboxaldehyde) protein quantification kit. Antimicrobial activity and biocompatibility of AMP-modified G-PDMS were demonstrated both *in vitro* and *in vivo*. Overall, this study provides new insights into the use of CVD graphene with AMP modification for the prevention and treatment of bacterial infections associated with biomedical devices.

Experimental

Materials

CVD graphene coated polydimethylsiloxane (G-PDMS) was purchased from 2D Carbon Tech (Changzhou, China). Peptides were synthesized by GL Biochem (Shanghai, China), with purity validated using reverse-phase high-performance liquid chromatography (RP-HPLC) to be >95%. Other reagents were purchased from Sigma-Aldrich (St. Louis, MO) and used without further purification. All bacteria strains and mammalian cell lines were obtained from American Type Culture Collection (Manassas, VA).

Preparation of AMP-modified G-PDMS

G-PDMS was oxidized using the modified Hummer's method. In brief, a mixture of 85% phosphoric acid (2 ml), 98% sulfuric acid (3.5 ml) and potassium permanganate (50 mg) was applied onto the graphene surface for 20 s then rinsed twice in DI water. The mixture only reacted with graphene coating. PDMS substrate did not contact with the mixture. The oxidized material was immersed in a solution of 5 mg/ml of sodium hydroxide and 5 mg/ml of sodium chloroacetate for 20 s then rinsed twice in DI water to convert the oxygen groups to carboxyl groups. To conjugate the AMPs onto graphene coating surface through amide bond, the activation of carboxyl groups from coating surface was performed using N-(3-Dimethylaminopropyl)-N'-ethylcarbodiimide hydrochloride (EDC) : N-Hydroxysuccinimide (NHS) = 1 : 3 as activators. The mixture of EDC and NHS was prepared in 1× Phosphate Buffered Saline (PBS). EDC was added into 1×PBS with pH5.5 then NHS was added. The carboxylate material was immersed in the mixture of EDC and NHS for 30 min. Afterward, the materials were transferred into peptide solution (0.2 mg/ml, pH 7.2) for 1 h then rinsed twice in DI water. The material was dry in the fume hood then kept in the dry cabinet.

Surface Characterisation

Atomic Force Microscopy (AFM) measurements were performed on Bruker Dimension ICON with controller Nanoscope V (Billerica, Massachusetts, US). The surface roughness was measured by the Nanoscope V software during AFM image collection. Images were collected using Nanoscope

9.7 and analyzed using NanoScope Analysis 2.0. The surface microstructure was observed using scanning electron microscope (SEM). Materials were firstly subjected to gold coating using Leica EM ACE200 (Wetzlar, Germany). Viewing of the samples was performed using JEOL JSM-6701F (Tokyo, Japan). Fourier transform infrared (FTIR) spectra were obtained on the Perkin Elmer Spectrum 100 (Wellesley, MA). The chemical states of composing elements of AMP-modified CVD graphene coating were investigated by XPS using Kratos AXIS Ultra DLD (Kratos Analytical Ltd., Manchester, UK). The binding energy values of XPS lines were calibrated using the C 1s peak at 284.5 eV as reference. AMP-modified G-PDMS samples were processed using CBQCA protein quantification kit and placed on coverslip then imaged using FV1000 TIRF inverted laser scanning confocal microscope (Olympus, Tokyo, Japan). Images were processed using ImageJ (National Institutes of Health, Bethesda, MD). The CBQCA Protein Quantification Kit (Molecular Probes, Eugene, OR) was used to quantify the conjugated AMP on G-PDMS. Material was cut into 0.5 x 0.5 cm² pieces and placed in 96-well black plate with 0.1 M sodium borate (pH 9.3). For the calibration curve, a solution of 50 µg/ml of each peptide was used to prepare a serial dilution (0.5, 0.75, 1, 1.5, 2, 3 µg) in reaction buffer. Then, 5 µl of 20 mM KCN and 10 µl of 2 mM CBQCA were added per well and mixed well. After incubation at room temperature (120 rpm, 1 h, in the dark), the fluorescence emission was measured (550/465 nm) using TECAN Infinite M200 (Männedorf, Switzerland). All samples were measured in triplicates.

Wettability

Video contact angle system VCA-Optima TM (AST Products, Inc., Billerica, MA) was used to measure the static contact angle on the coating surfaces to evaluate the effect of graphene coating on wettability. DI water and glycerol (2 µL droplet) were used as solvent for measurement. All samples were measured in triplicates.

The surface energy was calculated from the contact angle values with water and glycerol, using equation (1):

$$\gamma_L(\cos \theta + 1) = 2(\gamma_S^d \gamma_L^d)^{\frac{1}{2}} + 2(\gamma_S^p \gamma_L^p)^{\frac{1}{2}} \quad (1)$$

where θ is contact angle, γ_L is the total SFE of the liquid, γ_L^d is the dispersive SFE of the liquid, γ_L^p is the polar SFE of the liquid, γ_S^d is the dispersive SFE of the surface, γ_S^p is the polar SFE of the surface. γ_S is the total SFE of the surface, which is equal to $\gamma_S^d + \gamma_S^p$.

Biofilm Prevention Efficiency against Four Types of Pathogenic Microbes

P. aeruginosa PAO1 and *S. aureus* ATCC 29737 were cultured in Tryptic Soy Broth (TSB) and Luria-Bertani (LB) Broth respectively, supplemented with 10% fetal bovine serum (FBS), at 37°C under constant shaking for 6 to 12h. The microbe density was diluted to obtain an optical density reading at wavelength of 600 nm (OD₆₀₀) of 0.07 on a TECAN microplate reader (Männedorf, Switzerland), then further diluted 100-fold



to 10^6 colony-forming units (CFU)/mL for the starting culture. 1 cm × 1 cm polymer samples were sterilized under UV for 30 min, then incubated with bacteria culture in 24-well plate at 37°C for 48 h to allow biofilms to form. *Mycobacteroides abscessus* (*M. abscessus*) ATCC 19977 was cultured in Middlebrook 7H9 Broth supplemented with ADC enrichment (37°C, 12 to 24h). The culture was diluted to 10^7 CFU/ml for starting culture. Similarly, material samples were incubated with *M. abscessus* in 24-well plate at 37°C for 7 days. *Candida albicans* (*C. albicans*) was inoculated on Sabouraud Dextrose agar (Neogen) and incubated at 37°C for 24 to 48 h. Then, one loopful of colony was harvested and evenly suspended in 1×PBS to wash twice. The microbes were then resuspended in RPMI-1640 supplemented with 10% FBS. 2×10^6 CFU/ml were seeded into 24-well plate and incubated with materials at 37°C for 48 h to allow biofilm to form. After incubation, the culture media was removed. Material samples were rinsed with PBS, then transferred to fresh PBS. Biofilm was extracted by cycles of vortexing and sonication for 1 min each at room temperature. Then, the supernatant containing detached cells were plated on agar plates. All plates were incubated at 37°C for 12-24h (*P. aeruginosa*, *S. aureus* and *C. albicans*) or 3-5 days (*M. abscessus*), then counted for colonies.

LIVE/DEAD Biofilm Viability Assay

To visualize the viability of bacteria within biofilm on surfaces, a LIVE/DEAD biofilm viability kit (Invitrogen) using SYTO9 and propidium iodide (PI) was employed. After incubation with the microbes, the culture media was removed, and the material samples were rinsed with PBS. After cells were fixed with 4% formaldehyde, samples were stained following the manual provided by the manufacturer, then observed using confocal laser scanning biological microscope (CLSM) FV1000 and FV3000 (Olympus). 3D confocal images were processed using Imaris (Oxford, UK).

Cell Viability Assay

Cell viability was determined using the MTS assay kit. Briefly, 40,000 cell/well of human hepatocellular carcinoma (HepG2, ATCC HB-8065) or human umbilical vein endothelial (HUVEC, ATCC CRL-1730) were cultured for 24 h (37°C, 5% CO₂). MTS reagents were added following the kit instructions, and absorbance was recorded at 490 nm. Cells were incubated without any materials as positive control, and with 0.1% triton-x as negative control. The normalized cell viability of each material was calculated using equation (2).

$$\text{Normalized cell viability} = \frac{\text{sample abs} - \text{negative control abs}}{\text{positive control abs} - \text{negative control abs}} \quad (2)$$

HepG2 cells were grown (37 °C, 5% CO₂) in high-glucose Dulbecco's Modified Eagle Medium (DMEM) supplemented with 10% heat-inactivated FBS (HyClone), 1% Penicillin-Streptomycin. HUVECs were grown in endothelial cell growth medium at 37 °C in 5% CO₂ incubator.

Hemolysis Assay

Blood was collected from healthy donors based on protocol approved by the Institutional Review Board (IRB) (Protocol No. H-20-025). Red blood cells (RBCs) were separated by centrifugation (1200 rpm, 10 min), washed once with same volume 1×PBS, and diluted to 10% v/v. Graphene samples of dimension 1 cm × 1 cm were equilibrated in 24-well plate containing 500 μl of PBS at 37 °C for 1 h. 500 μl of 10% v/v RBC suspension was then added into the well. The final concentration of RBC in each well is 5% v/v. Equal volume of PBS and 2% Triton-X 100 were added as negative and positive controls, respectively. After incubation (37 °C, 1 h), RBC suspensions were centrifuged (1200 rpm, 10 min). Aliquots (50 μl) of supernatant were transferred into a new 96-well plate and diluted with 50 μl of PBS. The absorbance at 540 nm was measured using Tecan, then normalized using equation (3).

$$\text{Normalized hemolysis} = \frac{\text{sample abs} - \text{negative control abs}}{\text{positive control abs} - \text{negative control abs}} \quad (3)$$

Tube Formation Assay

To investigate the angiogenic effects of CVD graphene coating on HUVECs, a Matrigel-based tube formation assay was conducted. Matrigel was first thawed at 4 °C overnight. Using cooled pipette tips, 100 μl of Matrigel was added on top of the coating surface. The plate was incubated (37 °C, 30 min) to enable gelation prior to the assay. Next, 80,000 cell/well of HUVECs were seeded into Matrigel-coated well. After incubation at 37 °C for 4, 8 and 12 h, images of the formation of capillary-like structures were captured using the Ti-S microscope with imaging system (Nikon) at 4× magnification. The number of loops formed by the connected cells in randomly selected fields were manually counted. The experiment was conducted in duplicates and repeated three times.

Antimicrobial activity determination

Bacteria culture in mid-log phase was diluted to 10^6 CFU/ml for seeding. 1×1 cm² material samples were sterilized under UV for 30 min, then incubated with diluted bacteria culture in a 24-well plate (37°C, 48 h) to allow biofilm to form. After rinsing with PBS, biofilm was extracted using vortexing-sonication-vortexing cycles. The supernatant containing detached bacteria cells was plated on agar plate. *P. aeruginosa* was plated on Tryptic Soy Agar. *S. aureus* was plated on LB agar. All plates were incubated at 37°C for 12-24h, then counted for colonies. Results are reported as mean ± SD of three independent experiments performed in duplicates.

The supernatant containing detached bacteria cells was transferred into 96-well. XTT assay kit (Abcam, Cambridge, UK) was used to evaluate the metabolic activity of bacteria following the manufacturer's protocol. All the values have been reported as the mean ± SD of three independent experiments performed in duplicates.

Protein deposition

After 1×1 cm² material samples were immersed in PBS for 1 h, they were soaked in 1 ml of artificial tear fluid containing 2.5 mg/ml of Lysozyme, 0.1 mg/ml Bovine Serum Albumin, 0.5 mg/ml of mucin and 0.3 mM of calcium chloride, and incubated



for 16 h at 37 °C. This deposition period simulates a typical duration of CL usage in a day. Afterward, the sample was rinsed three times with PBS, and subsequently placed in 15 ml Falcon tube with 1 ml of 1xPBS containing 1 wt % of sodium dodecyl sulfate (SDS, Sigma), shaking 120 rpm for 60 min. The concentration of deposited proteins on material surface were evaluated using Bicinchoninic acid (BCA) method (Micro BCA Protein Assay Kit, ThermoFisher) at 562 nm based on the manufacturer's instructions. All samples were measured in triplicates.

Ex vivo Porcine Skin Model of *P. aeruginosa* infection

Porcine skin was obtained from SingHealth (Singapore). The skin was washed thoroughly with sterile water and chlorhexidine after harvesting, then soaked in sterile saline stored at 4 °C prior to use. After removing the hair and fat layer, the porcine skin was biopsied into round pieces of 8 mm diameter, sterilized by dipping in 70% ethanol, and rinsed with sterile PBS. The skin sample was then dried with sterile gauze and placed into a 12-well plate. Each skin sample was inoculated with 10⁶ CFU/ml of *P. aeruginosa* culture in THB. 1x1 cm² material samples were then applied onto the skin surface and incubated at 37 °C for 24 h in a humidified chamber. To quantify the remaining viable bacteria, the skin surface was scraped three times using an inoculum loop after removing the materials. The collected bacteria were suspended in PBS and diluted serially, then added to TSA plates. After overnight incubation at 37 °C, and the colonies were counted.

To visualize bacteria on the skin surface, the skin sample was processed for SEM imaging. After incubation, the materials were removed, and the skin samples were gently washed with PBS once. Then, the skin samples were fixed in 4% formaldehyde at 4°C overnight. After fixation, samples were rinsed with PBS, and then immersed in 1% OsO₄ for 1.5 h. After aspirating OsO₄, samples were washed with water and left for 10 min twice, following the dehydration with a series of ethanol solutions (25% for 50 min, 50% for 50 min, 75% for 20 min, 90% for 20 min twice, 100% for 20 min three times). The skin samples were then subjected to critical point drying using Leica EM CPD300 (Wetzlar, Germany), followed by sputter gold coating using Leica EM ACE200 (Wetzlar, Germany). Finally, the viewing of samples was performed using JEOL JSM-6701F (Tokyo, Japan). Images were processed using ImageJ (National Institute of Health, Bethesda, MD).

To evaluate the integrity of skin structure, hematoxylin and eosin (H&E) staining was performed. After incubation, the skin samples were washed with PBS and then fixed in 4% paraformaldehyde at 4°C for 48-72 h. Then, the tissue samples were transferred to 15% sucrose in PBS until tissues sink (6-12 h) and then 30% sucrose in PBS overnight until tissues sink, following cryo-embedding. The embedded samples were sectioned and stained, then imaged with TissueFAXS Silde Scanner (TissueGnostics, Vienna, Austria).

In vivo Biocompatibility

PDMS, G-PDMS and BTT6-G-PDMS were cut into a round shape (diameter 8 mm) as CLs. CLs were worn by rabbits daily for up to at least 10 hours per day for 5 days. Slit-lamp (SL), Anterior Segment

Optical Coherence Tomography (AS-OCT) and Intraocular pressure (IOP) were measured daily before lens application. Rabbits with CLs wearing were checked hourly or more frequently. 3 different CLs material with n = 2-3 animals per group (PDMS n = 4 eyes, G-PDMS n = 6 eyes, BTT6-G-PDMS n = 6 eyes). CLs were applied on healthy Rabbits (Male, NZW rabbits weighing at least 3 kg each). Used CLs were removed daily and the protein deposition was measured by the BCA method. This safety and biocompatibility study on 3 different CLs on the rabbit model was performed at Singapore Eye Research Institute (SERI) under the protocol (Ref.2018/SHS/1447) approved by Institutional Animal Care and Use Committee (IACUC)

Statistical Analysis

Data was analyzed by one-way ANOVA test using Prism 7 (GraphPad, La Jolla, CA, USA). All the values have been reported as the mean ± standard deviation (SD). * $p < 0.05$, ** $p < 0.01$, *** $p < 0.001$, and **** $p < 0.0001$ indicates statistical significance.

Results and Discussion

Surface Characterisation of CVD Graphene Coating

As observed using AFM (Fig. S1(a)), G-PDMS had an average surface roughness of 2.05 nm, G-PDMS was generally smooth with minimal contrast in the height images. Fig. S1(b) shows the corresponding phase image which is indicative of a microlayer pattern. Through the contrast of the image, the bright and dark areas indicate the high- and low-density of material surface respectively. The CVD graphene coating appeared smooth without fixed microlayer pattern and unambiguous assignment of hard and soft areas²³.

Wettability of surfaces is typically indicative of antifouling effect²⁴. Surfaces capable of resisting microbial fouling are commonly hydrophilic, owing to high hydration and surface energy. A tight water layer can act as a physical and free energy barrier to prevent adhesion by foulants²⁵. In contrast, low surface energy of hydrophobic surface provides self-cleaning potential²⁴. The contact angle of G-PDMS was <90° (Table 1), while the contact angle of uncoated PDMS was >90°. This suggests that CVD graphene coating rendered the polymer surface more hydrophilic. This was further supported by comparing the surface free energy (SFE) and its polar (γ^p) and dispersive (γ^d) components of G-PDMS and PDMS (Table 1).

Table 1. Static contact angle and surface energy components of different polymer surfaces

Samples	Static contact angle, θ (deg)		Surface free energy (mJ/m ²)		
	θ^w	θ^g	γ_s^d	γ_s^p	γ_s
PDMS	118.4 ± 0.8	112.0 ± 0.5	5.7	1.2	6.9
G-PDMS	78.0 ± 1.3	76.7 ± 0.8	6.3	20.4	26.7

θ^w : contact angle of distilled water, θ^g : contact angle of glycerol, γ_s : total SFE of the surface, γ_s^p : polar SFE of the surface, γ_s^d : dispersive SFE of the surface



Antifouling Activity and Biocompatibility of CVD Graphene Coating

To investigate the antifouling function of G-PDMS, we tested representative strains of four types of microbes – Gram-negative *P. aeruginosa*, Gram-positive *S. aureus*, mycobacteria *M. abscessus*, and yeast *C. albicans*. Biofilms formed by these microbes are commonly responsible for device-related infections^{5,26–30}.

G-PDMS was only effective at reducing the colony density of *P. aeruginosa* and *C. albicans* (Fig. 1(a-c)), resulting in a lack of intact biofilm formation as visualized with confocal microscopy in Fig. 1(d) and 1(g). *S. aureus* biofilm on G-PDMS is thick and dense shown in Fig. 1 (e). Only a few dead bacteria (bright ellipse stained by PI in red colour) distributed in the biofilm (Fig. S9). The data suggests that CVD graphene coating on PDMS exhibits strain-selective antifouling effect, and that activity spectrum of the coating can vary depending on the choice of polymer material.

To evaluate the effect of CVD graphene coating on the intrinsically biocompatible PDMS, we measured the cytotoxicity of G-PDMS against epithelial HepG2 and endothelial HUVEC cell lines using MTS assay kit, and hemocompatibility against human RBCs. Fig. S2(a) showed that the mammalian cell viability on CVD graphene-coated substrate was comparable to the uncoated polymers. Notably, the viability of HUVECs on G-PDMS (>90%) was clearly higher than on PDMS. In addition, negligible hemolysis was observed with both PDMS and G-PDMS (Fig. S2(b)). Overall, these results support a lack of *in vitro* toxicity of CVD graphene-coated materials.

Effect of CVD graphene coating on cell differentiation

Based on prior reports that GO and rGO can induce angiogenesis^{31–36}, we investigated whether CVD graphene coating also display a similar effect. Tube formation assay is a fast and quantitative technique to assess impacts on angiogenesis process by evaluating the capillary-like structures formed by endothelial cells^{37–39}.

As shown in Fig. 2(b), HUVEC cells cultured on G-PDMS exhibited significantly higher number of loops than those on uncoated substrate after 4 h, indicating that CVD graphene coating can enhance angiogenesis. Endothelial cells first attach to the matrix (i.e., Matrigel) and migrate towards each other, then connect and align to form capillary-like tubes³⁷. The tubes maturation process continues until the cells undergo apoptosis, leading to tube destruction and detachment. Hence, our results seemed to suggest that the maturation of tubes on G-PDMS is faster than uncoated PDMS. We also observed that endothelial cells differentiated morphologically to form tubes shown in Fig. 2(a). Overall, CVD graphene coating displays multifunctionality, not only preventing biofilm formation but also promoting tissue regeneration and may be applicable in clinical conditions such as wound healing, implant integration, cardiovascular stents, nerve regeneration, bone repair, and tissue engineering scaffolds.

Synthesis and characterization of AMP-modified G-PDMS

We previously reported the design of three synthetic AMPs with potent antimicrobial activity against Gram-negative clinical isolates (i.e. BTT2, BTT4 and BTT6)²², which were selected for conjugation to the CVD graphene coating. BTT2, 4, and 6 are peptides that adopt random coiled structures in aqueous environments. Upon encountering lipopolysaccharides (LPS), the secondary structure of these peptides undergoes a conformational change to anti-parallel β -sheet and β -turn. Due to the presence of LPS in the outer membrane of Gram-negative bacteria, BTT peptides exhibit selective activity against Gram-negative bacteria. When BTT peptides come into contact with outer membranes, they undergo further conformational changes and damage the inner membrane in a concentration-dependent manner. When these peptides are covalently conjugated to a solid surface, they may also adopt a random coil structure. Upon bacterial attachment and contact with the peptide, the conjugated peptides transform into a beta-hairpin structure, ultimately disrupting the bacterial membrane and killing the bacteria. However, there is currently no technique available to determine the secondary structure of these peptides when conjugated to a solid surface. A natural AMP with broad-spectrum activity, Magainin 1^{40,41}, was also tested in this work. As known from literature, Magainin 1 can disrupt cell membranes, but its mechanism against microorganisms is not fully clear⁴². It lacks a stable conformation in water but forms amphipathic α -helix in membranes⁴⁰. The AMP was covalently conjugated onto CVD graphene coating through a three-step process as shown in Fig.3. FTIR was used to monitor the outcome of each synthesis step (Fig. 4(a)). The presence of characteristic adsorption peaks at 3200 cm^{-1} (stretching vibration of -OH), 1700 cm^{-1} (stretching vibration of C=O), and 1580 cm^{-1} (stretching vibration of C=C) indicate the presence of carboxyl groups, hydroxyl groups, carbonyl groups and C=C functional groups in oxidized CVD graphene coating. Carboxylated CVD graphene coating showed a stronger adsorption band at 1600 cm^{-1} , indicating the formation of carboxylate moieties COO⁻. Following the conjugation of AMP, two strong characteristic bands appeared at 3300 cm^{-1} (stretching vibration of N-H) and 1660 cm^{-1} (stretching vibration of -CO-NH-) with small peaks at 2900 cm^{-1} (stretching vibration of -CH₂-) intensified, thus confirming the formation of AMP-modified CVD graphene coating. XPS C 1s and N 1s narrow scan were also performed to verify the success of AMP conjugation to G-PDMS (Fig.4(b-c)). XPS C 1s spectrum showed the presence of C-C (284.5 eV), C-O (286.3 eV), N-C=O (288.3 eV) and O-C=O (289.0 eV) moieties. According to the XPS N 1s spectrum, there were two types of Nitrogen bond, N-C=O at 399.7 eV and C-NH₂ at 399.4 eV, which suggest the formation of amide bonds between amino groups in peptides and carboxyl groups in carboxylated CVD graphene.

Surface characterization of AMP-modified coating

We next quantified the amount of AMP conjugated onto G-PDMS. Although synthesized using similar parameters, we observed variation in the degree of peptide conjugation to the substrates (Fig. 5(a)), with BTT6 displaying the highest



conjugation efficiency and BTT2 the lowest. Previously shown to be the only BTT peptide to form fibrils in response to bacterial membranes²², BTT2 might have aggregated in the reaction buffer, thus resulting in fewer free molecules available for covalent bonding with CVD graphene. Admittedly, the CBQCA method has limitations in quantifying conjugated peptides, primarily due to potential discrepancies between the quantity of unreacted amino groups on conjugated AMPs versus the peptides in solution used for preparing the calibration curve. Nevertheless, this methodology has provided valuable preliminary semi-quantitative data that informed the current research. Future research directions will implement more accurate analytical techniques to overcome this limitation.

The confocal microscopy images showed that all four peptides formed irregularly distributed clumps on G-PDMS (Fig. 5(b)). PDMS alone showed moderate hydrophobicity (Table 1), which could have led to uneven distribution of oxygen groups found on the CVD graphene coating. This in turn directed the non-uniform conjugation pattern of peptides onto the graphene surface. SEM images further supported the clumping of peptides resulting in rough material surface compared to unmodified substrates (Fig. 5(c)).

High optical transparency is a desirable attribute in the design of some medical devices, such as being essential to the visual performance and optical quality of CLs^{43,44}. As shown in Fig. S4, all AMP-modified G-PDMS maintained excellent transparency (>99.5%), which was comparable to the G-PDMS and PDMS, suggesting that the observed peptide clumps did not undermine the overall transparency. In contrast, AMP conjugation clearly lowered the static water contact angle (Table 2), indicating greater hydrophilicity of the coatings due to the highly cationic peptides. Compared to unmodified CVD graphene coating, AMP-modified surface displayed more protein deposition (Fig. S5), which was still lower than the amount previously reported for commercial devices^{45–47}.

Table 2. Static water contact angle of plain substrate, unmodified and AMP-modified CVD graphene coated surface.

Samples	Contact angle, θ (degree)
PDMS	118.40 \pm 0.80
G-PDMS ^a	79.43 \pm 1.34
BTT2-G-PDMS ^{a,b}	47.60 \pm 2.41
BTT4-G-PDMS ^{a,b}	41.05 \pm 4.73
BTT6-G-PDMS ^{a,b}	40.37 \pm 2.81
Magainin1-G-PDMS ^{a,b,c}	34.22 \pm 5.38

Data are shown as mean \pm SD. Data was analyzed by one-way ANOVA test with post-hoc test (Tukey's multiple comparisons test). ^a: There is significant difference with PDMS ($n = 3$, $p < 0.0001$). ^b: There is significant difference with G-PDMS ($n = 3$, $p < 0.0001$). ^c: There is significant difference with BTT2-G-PDMS ($n = 3$, $p < 0.01$).

In vitro Antimicrobial Activity of AMP-modified G-PDMS

All AMP-modified G-PDMS showed antimicrobial activity against *P. aeruginosa* (Fig. 6). The colony count after treatment with AMP-modified surface was significantly lower than with

unmodified surface (Fig. 6(a)). This result was supported by XTT assay which showed lower metabolic activity of the bacteria on AMP-modified surface. Confocal images showed that *P. aeruginosa* cells found on the AMP-modified surface were mostly dead as stained by the red PI and no biofilm structure could be observed. In contrast, dense intact biofilms could be seen on the unmodified CVD graphene surface (Fig. 6(c)) and plain substrate (Fig. S6).

Meanwhile, *S. aureus* formed intact biofilm with high cell viability on all AMP-modified G-PDMS (Fig. S7), which might be explained by the Gram-negative-selective antimicrobial profile of BTT peptides²². Although Magainin 1 is a broad-spectrum AMP, it was equally ineffective in preventing *S. aureus* growth following surface conjugation. These findings suggest that conjugation to material surface may alter the antimicrobial profile of AMP, which is an unexpected finding.

In vitro Cytotoxicity of AMP-modified G-PDMS

To evaluate cytotoxicity of AMP-modified graphene coating as potential CLs coating, cell viability of human corneal epithelia (HCE) cell and human corneal fibroblast (Fb) cell was determined using MTS assay. After 24 h incubation with unmodified and AMP-modified G-PDMS samples of dimension 1 cm \times 1 cm, the results showed that cell viability of all AMP-modified groups was comparable to unmodified groups, suggesting that AMP modification did not induce cytotoxicity shown in Fig. 7(a-b). The amount of conjugated AMP per cm² in this study can be considered as safe dosage. From Fig. 7(c-d), the HCE and Fb cells incubated with AMP-modified and unmodified G-PDMS maintained normal morphology compared to controls. Cell viability was measured after the removal of materials.

Evaluation of antimicrobial efficacy on *P. aeruginosa*-infected skin

We next established the antimicrobial efficacy of the coating on an *ex vivo* skin infection model, following a reported method with modifications⁴⁸. After 24 h of treating *P. aeruginosa*-infected porcine skin samples with the materials, bacteria were collected from the skin surface and quantified through colony counting. AMP-modified G-PDMS resulted in significantly lower bacteria attachments compared to plain substrate and unmodified CVD graphene, with 2- to 3-log reduction in CFU/cm² (Fig. 8(a)). Visualization of the skin surface using SEM supported that AMP-modified CVD graphene coating was effective at preventing biofilm formation with only highly scattered individual bacterial cells, whereas a dense and thick biofilm could be seen on the negative control skin surface or treated with uncoated PDMS (Fig. 8(c)). G-PDMS-treated skin surface also carried biofilm clumps and appeared damaged. At a higher magnification of 10,000 \times (Fig. 8(d)), bacteria on infected skin without treatment or treated with non-peptide coatings displayed smooth and intact membrane surfaces. Meanwhile, bacteria on BTT6-G-PDMS treated skin surface showed membrane blebs indicative of disruption. Taken together, these observations support the superior anti-biofilm and antimicrobial activity of AMP-modified CVD graphene.



To evaluate the integrity of skin tissues after treatment with the materials, skin tissues were subjected to H&E staining. While hematoxylin stains nuclei in blue, eosin stains cytoplasm and most connective tissues in pink. Therefore, epidermis is stained by both. In Fig. 9, intact skin showed clear boundary between epidermal and dermal layers. The infected skin without treatment and treated with PDMS and G-PDMS was damaged with no discernible nuclei among dermal tissues. There were multiple fuzzy areas indicative of bacteria biofilms. Colonization by bacteria led to the destruction of skin. In contrast, treatment with AMP-modified G-PDMS helped maintain skin integrity comparable to that of uninfected skin. Negligible bacteria count was observed on top of the epidermis with peptide treatment.

In vivo Biocompatibility

Lastly, we examined the *in vivo* biocompatibility of AMP-modified CVD graphene coating on rabbit eyes through eye morphology, IOP, and CCT. We selected BTT6-G-PDMS as the representative coating by virtue of suitable wettability, light transmittance, protein deposition, distinct antimicrobial activity and excellent biocompatibility. PDMS and G-PDMS were tested as controls. No apparent discomfort, irritation, or redness during wear and after removal was observed among the rabbits (Fig. S8). Normal IOP of 10–21 mmHg was maintained throughout five continuous changing cycles, as shown in Fig. 10(a). CCT did not increase after application of all materials, indicating excellent biocompatibility (Fig. 10(b) and (e)). SL images showed an absence of hyper-reflective materials and non-edematous (Fig. 10(d)), which confirmed excellent biocompatibility. BTT6-G-PDMS displayed low protein deposition as well (Fig. 10(c)). Overall, these results demonstrated excellent biocompatibility of AMP-modified CVD graphene coating, which further promotes its appeal for application on biomedical devices.

Conclusions

In summary, CVD graphene coating with AMP modification is a promising strategy to prevent bacterial infections caused by biofilm formation on biomedical device surface. In addition, the material exhibited effective antimicrobial and anti-biofilm activity, and excellent biocompatibility. This study highlights the potential of CVD graphene coating and AMP-modified CVD graphene coating on biocompatible materials to minimize bacterial infection and prevent the occurrence of infections associated with biofilms.

Author contributions

Xiao Zhu conceptualized, designed, performed experiments, wrote and edited the manuscript. **Nhan Dai Thien Tram** assisted in the experiments and edited the manuscript. **Dhanya Mahalakshmi Murali** assisted in the experiments. **Veluchamy Amutha Barathi**, **Mayandi Venkatesh** and **Rajamani Lakshminarayanan** assisted the *in vivo* biocompatibility evaluation, critically discussed the results

and reviewed the manuscript. **Pui Lai Rachel Ee** conceptualized, designed, edited and supervised the work. DOI: 10.1039/D5NR01674F

Conflicts of interest

There are no conflicts to declare.

Data availability

The data supporting this article have been included as part of the Supplementary Information.

Acknowledgements

The research work described in this manuscript was conducted with facilities provided by the National University of Singapore. The authors gratefully acknowledge the financial support provided by Ministry of Education Academic Research Grant (A-0004347-00-00) and Singapore Ministry of Health's National Medical Research Council under its Individual Research Grant Scheme (NMRC/OFIRG/0026/2016) awarded to P.L.R.E., Singapore Ministry of Health's National Medical Research Council under its Open Fund – Individual Research Grant (R1875/3/2022) awarded to R.L.

We would like to appreciate the Electron Microscopy Unit and the Confocal Microscopy Unit (Yong Loo Lin School of Medicine, National University of Singapore) for the assistance in microscopic imaging. We'd like to acknowledge the Histology Core Facility (Life Sciences Institute, National University of Singapore) for assistance in H&E staining of porcine skin samples. We'd like to thank the Department of Chemical and Biomolecular Engineering (College of Design and Engineering, National University of Singapore) for assistance in XPS and AFM measurement.

References

- 1 S. S. Magill, J. R. Edwards, W. Bamberg, Z. G. Beldavs, G. Dumyati, M. A. Kainer, R. Lynfield, M. Maloney, L. McAllister-Hollod, J. Nadle, S. M. Ray, D. L. Thompson, L. E. Wilson and S. K. Fridkin, *N. Engl. J. Med.*, 2014, **370**, 1198–1208.
- 2 N. Khardori and M. Yassien, *J. Ind. Microbiol.*, 1995, **15**, 141–147.
- 3 H. Wei, X. Song, P. Liu, X. Liu, X. Yan and L. Yu, *Biomater. Adv.*, 2022, **135**, 212739.
- 4 D. M. Siddiq and R. O. Darouiche, *Nat. Rev. Urol.* 2012 **96**, 2012, **9**, 305–314.
- 5 G. E. Pierce, *J. Ind. Microbiol. Biotechnol.*, 2005, **32**, 309–318.
- 6 S. Veerachamy, T. Yarlagadda, G. Manivasagam and P. K. Yarlagadda, *Proc. Inst. Mech. Eng. Part H J. Eng. Med.*, 2014, **228**, 1083–1099.
- 7 R. Vasudevan, *J. Microbiol. Exp.*, , DOI:10.15406/jmen.2014.01.00014.
- 8 C. Liu, J. Guo, X. Yan, Y. Tang, A. Mazumder, S. Wu and Y.



- Liang, *Environ. Rev.*, 2017, **25**, 225–244.
- 9 M. E. Foo and S. C. B. Gopinath, *Biomed. Pharmacother.*, 2017, **94**, 354–361.
- 10 A. Lukowiak, A. Kedziora and W. Strek, *Adv. Colloid Interface Sci.*, 2016, **236**, 101–112.
- 11 M. D. Rojas-Andrade, G. Chata, D. Rouholiman, J. Liu, C. Saltikov and S. Chen, *Nanoscale*, 2017, **9**, 994–1006.
- 12 R. Kurapati, M. Vaidyanathan and A. M. Raichur, *RSC Adv.*, 2016, **6**, 39852–39860.
- 13 K. A. Whitehead, M. Vaidya, C. M. Liauw, D. A. C. Brownson, P. Ramalingam, J. Kamieniak, S. J. Rowley-Neale, L. A. Tetlow, J. S. T. Wilson-Nieuwenhuis, D. Brown, A. J. McBain, J. Kulandaivel and C. E. Banks, *Int. Biodeterior. Biodegradation*, 2017, **123**, 182–190.
- 14 C. Li, R. Ye, J. Bouckaert, A. Zurutuza, D. Drider, T. Dumych, S. Paryzhak, V. Vovk, R. O. Bilyy, S. Melinte, M. Li, R. Boukherroub and S. Szunerits, *ACS Appl. Mater. Interfaces*, 2017, **9**, 36665–36674.
- 15 S. Gurunathan, J. W. Han, A. A. Dayem, V. Eppakayala and J.-H. Kim, *Int. J. Nanomedicine*, 2012, **7**, 5901–14.
- 16 X. Li, W. Cai, J. An, S. Kim, J. Nah, D. Yang, R. Piner, A. Velamakanni, I. Jung, E. Tutuc, S. K. Banerjee, L. Colombo and R. S. Ruoff, *Science (80-.)*, 2009, **324**, 1312–1314.
- 17 A. Reina, X. Jia, J. Ho, D. Nezich, H. Son, V. Bulovic, M. S. Dresselhaus and K. Jing, *Nano Lett.*, 2009, **9**, 30–35.
- 18 G. Kalita and M. Tanemura, in *Graphene Materials - Advanced Applications*, InTech, 2017.
- 19 M. Saeed, Y. Alshammari, S. A. Majeed and E. Al-Nasrallah, *Mol. 2020, Vol. 25, Page 3856*, 2020, **25**, 3856.
- 20 J. Li, G. Wang, H. Geng, H. Zhu, M. Zhang, Z. Di, X. Liu, P. K. Chu and X. Wang, *ACS Appl. Mater. Interfaces*, 2015, **7**, 19876–19881.
- 21 I. Miranda, A. Souza, P. Sousa, J. Ribeiro, E. M. S. Castanheira, R. Lima and G. Minas, *J. Funct. Biomater.*, DOI:10.3390/JFB13010002.
- 22 N. D. T. Tram, V. Selvarajan, A. Boags, D. Mukherjee, J. K. Marzinek, B. Cheng, Z. C. Jiang, P. Goh, J. J. Koh, J. W. P. Teo, P. J. Bond and P. L. R. Ee, *Acta Biomater.*, 2021, **135**, 214–224.
- 23 M. Martínez-Ibáñez, N. S. Murthy, Y. Mao, J. Suay, M. Gurruchaga, I. Goñi and J. Kohn, *J. Biomed. Mater. Res. - Part B Appl. Biomater.*, 2018, **106**, 1138–1147.
- 24 A. M. C. Maan, A. H. Hofman, W. M. Vos and M. Kamperman, *Adv. Funct. Mater.*, 2020, **30**, 2000936.
- 25 S. Chen, L. Li, C. Zhao and J. Zheng, *Polymer (Guildf.)*, 2010, **51**, 5283–5293.
- 26 W. J. Kheir, H. Sheheitli, M. Abdul Fattah and R. N. Hamam, *Biomed Res. Int.*, 2015, 2015.
- 27 N. Safdar, C. J. Crnich and D. G. Maki, *Respir. Care*.
- 28 R. Gahlot, C. Nigam, V. Kumar, G. Yadav and S. Anupurba, *Int. J. Crit. Illn. Inj. Sci.*, 2014, **4**, 162.
- 29 N. Sabir, A. Ikram, G. Zaman, L. Satti, A. Gardezi, A. Ahmed and P. Ahmed, *Am. J. Infect. Control*, 2017, **45**, 1101–1105.
- 30 K. U. Zubair, A. H. Shah, A. Fawwad, R. Sabir and A. Butt, *Pakistan J. Med. Sci.*, 2019, **35**, 1664.
- 31 D. Xue, E. Chen, H. Zhong, W. Zhang, S. Wang, M. U. Joomun, T. Yao, Y. Tan, S. Lin, Q. Zheng and Z. Pan, *Int. J. Nanomedicine*, 2018, **13**, 5799.
- 32 P. X. Lai, C. W. Chen, S. C. Wei, T. Y. Lin, H. J. Jian, I. P. J. Lai, J. Y. Mao, P. H. Hsu, H. J. Lin, W. S. Tzou, S. Y. Chen, S. G. Harroun, J. Y. Lai and C. C. Huang, *Biomaterials*, 2016, **109**, 12–22.
- 33 S. Mukherjee, P. Sriram, A. K. Barui, S. K. Nethi, V. Veeriah, S. Chatterjee, K. I. Suresh and C. R. Patra, *Adv. Healthc. Mater.*, 2015, **4**, 1722–1732.
- 34 G. Cibecchini, M. Veronesi, T. Catelani, T. Bandiera, D. Guarnieri and P. P. Pompa, *ACS Appl. Mater. Interfaces*, 2020, **12**, 22507–22518.
- 35 A. K. Barui, A. Roy, S. Das, K. Bhamidipati and C. R. Patra, *Nanoparticles their Biomed. Appl.*, 2020, 147–189.
- 36 S. Chakraborty, T. Ponrasu, S. Chandel, M. Dixit and V. Muthuvijayan, *R. Soc. Open Sci.*, DOI:10.1098/RSOS.172017.
- 37 K. L. DeCicco-Skinner, G. H. Henry, C. Cataisson, T. Tabib, J. Curtis Gwilliam, N. J. Watson, E. M. Bullwinkle, L. Falkenburg, R. C. O'Neill, A. Morin and J. S. Wiest, *J. Vis. Exp.*, 2014, 51312.
- 38 M. L. Ponce, *Methods Mol. Biol.*, 2009, **467**, 183–188.
- 39 R. M. Brown, C. J. Meah, V. L. Heath, I. B. Styles and R. Bicknell, *Methods Mol. Biol.*, 2016, **1430**, 149–157.
- 40 S. J. Ludtke, K. He, W. T. Heller, T. A. Harroun, L. Yang and H. W. Huang, *Biochemistry*, 1996, **35**, 13723–13728.
- 41 M. Zasloff, B. Martin and H. C. Chen, *Proc. Natl. Acad. Sci.*, 1988, **85**, 910–913.
- 42 J. Michael Conlon, M. Mechkarska and J. D. King, *Gen. Comp. Endocrinol.*, 2012, **176**, 513–518.
- 43 N.-P.-D. Tran and M.-C. Yang, *Polymers (Basel)*, 2019, **11**, 944.
- 44 S. Wei, R. Yin, T. Tang, Y. Wu, Y. Liu, P. Wang, K. Wang, M. Mei, R. Zou and X. Duan, *ACS Nano*, 2019, **13**, 7920–7929.
- 45 S. E. Lee, S. R. Kim and M. Park, *J. Ophthalmol.*, DOI:10.1155/2017/5131764.
- 46 M. Kazemi Ashtiani, M. Zandi, P. Shokrollahi, M. Ehsani and H. Baharvand, *Polym. Adv. Technol.*, 2018, **29**, 1227–1233.
- 47 N. P. D. Tran and M. C. Yang, *J. Polym. Res. 2019 266*, 2019, **26**, 1–10.
- 48 N. Klubthawee, G. Bovone, B. Marco-Dufort, E. A. Guzzi, R. Aunpad, M. W. Tibbitt, N. Klubthawee, R. Aunpad, G. Bovone, B. Marco-Dufort, E. A. Guzzi and M. W. Tibbitt, *Adv. Healthc. Mater.*, 2022, **11**, 2101426.



ARTICLE

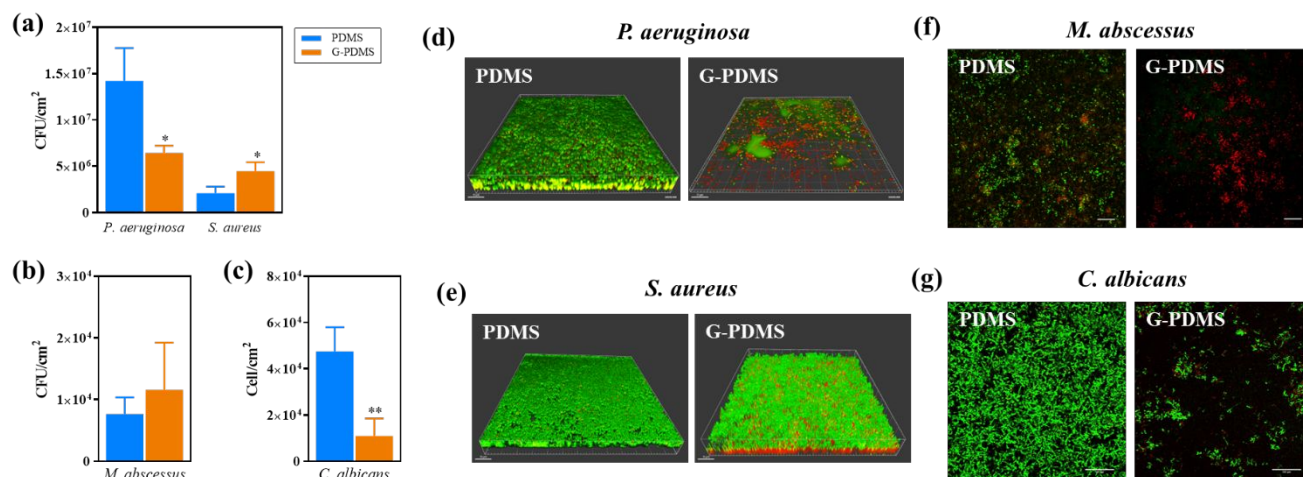


Fig. 1 Antifouling activity of CVD graphene coating on PDMS substrate in the presence of serum proteins against (a) *P. aeruginosa* and *S. aureus*, (b) *M. abscessus* shown in CFU/cm² and (c) *C. albicans* shown in cell/cm². Representative 3D confocal image of LIVE/DEAD biofilm stain against (d) *P. aeruginosa* and (e) *S. aureus*. Scale bar = 15 μm. Representative 2D confocal image of LIVE/DEAD biofilm stain against (f) *M. abscessus*. Scale bar = 20 μm. Representative 2D confocal image of LIVE/DEAD biofilm stain against (g) *C. albicans*. Scale bar = 100 μm. Data are shown as mean ± SD. Significant differences (n = 3, *: $p \leq 0.05$, **: $p \leq 0.001$) compared with PDMS substrate. Live bacteria was stained by SYTO9 in green colour, the dead bacteria was stained by PI in red colour.



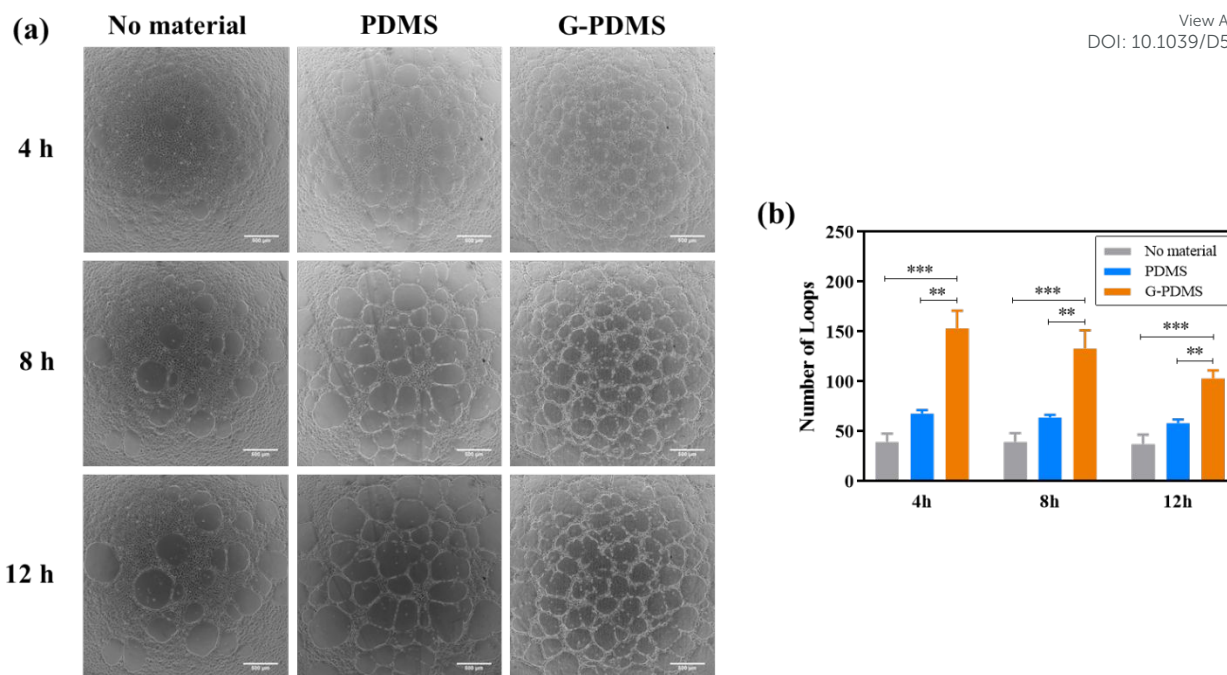


Fig. 2 Effect of CVD graphene coating on the HUVECs tube formation. (a) Representative light microscopy images of HUVECs inoculated on Matrigel in the absence or presence of polymer substrates for 4, 8 and 12 h. Scale bar = 500 μ m. (b) The number of loops formed by the HUVECs are plotted. Data are shown as mean \pm SD. Statistical significance was evaluated using one-way ANOVA ($n = 3$, **: $p \leq 0.01$, ***: $p \leq 0.001$).

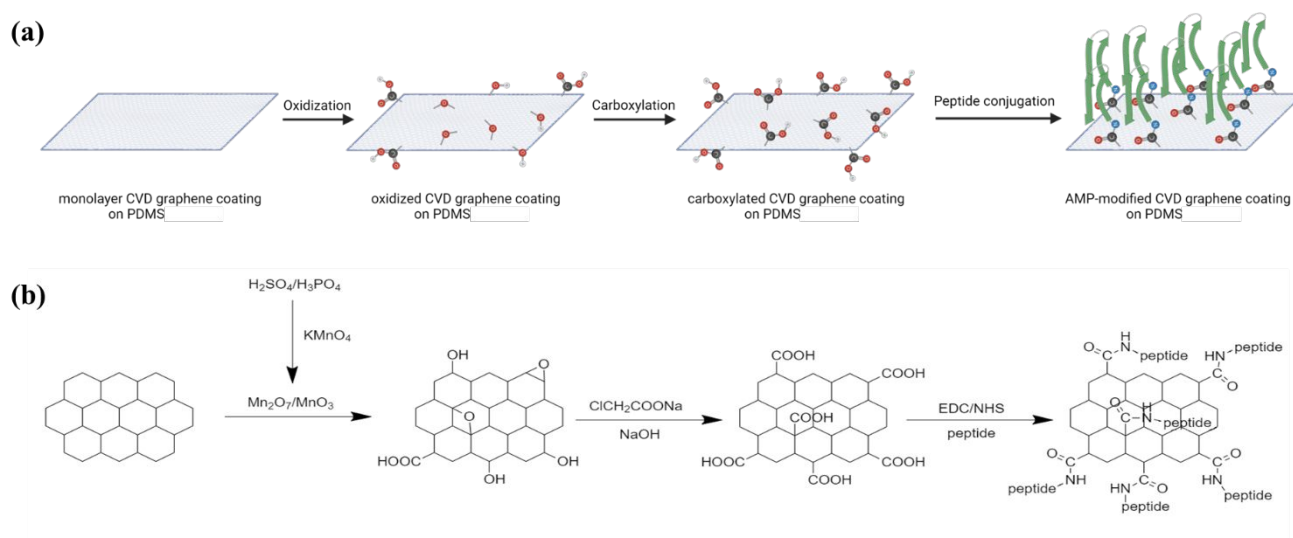


Fig. 3 Preparation of AMP-modified CVD graphene coating. (a) Schematic showing the covalent conjugation of AMP on CVD graphene coating. (b) Synthesis route of AMP-modified CVD graphene coating; step 1 oxidation to add oxygen functional groups, step 2 carboxylation to convert the oxygen functional groups to carboxyl groups, and step 3 peptide conjugation to conjugate the peptide through amide bond. Characterization of AMP-modified graphene coating.



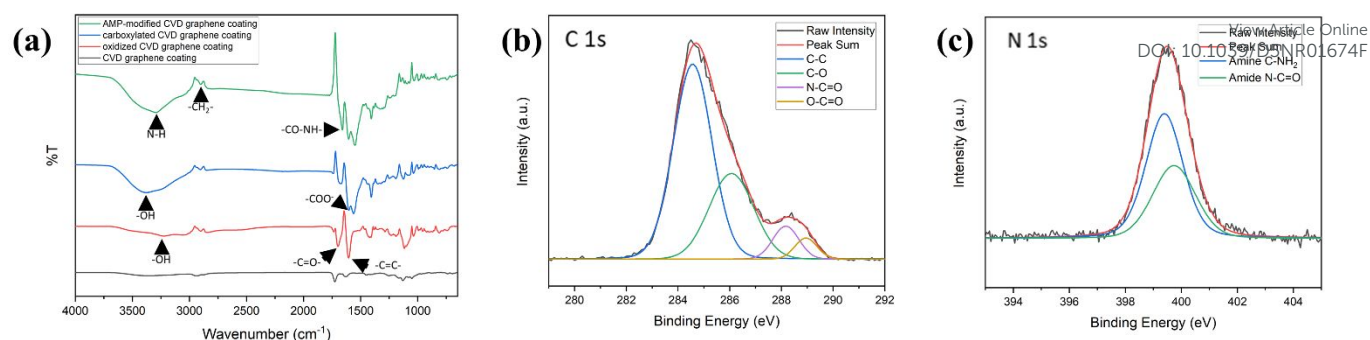


Fig. 4 Characterization of AMP-modified CVD graphene coating. (a) FTIR spectra of CVD graphene coating before and after each step. (b) XPS C 1s narrow scan and (c) XPS N 1s narrow scan of AMP-modified G-PDMS.



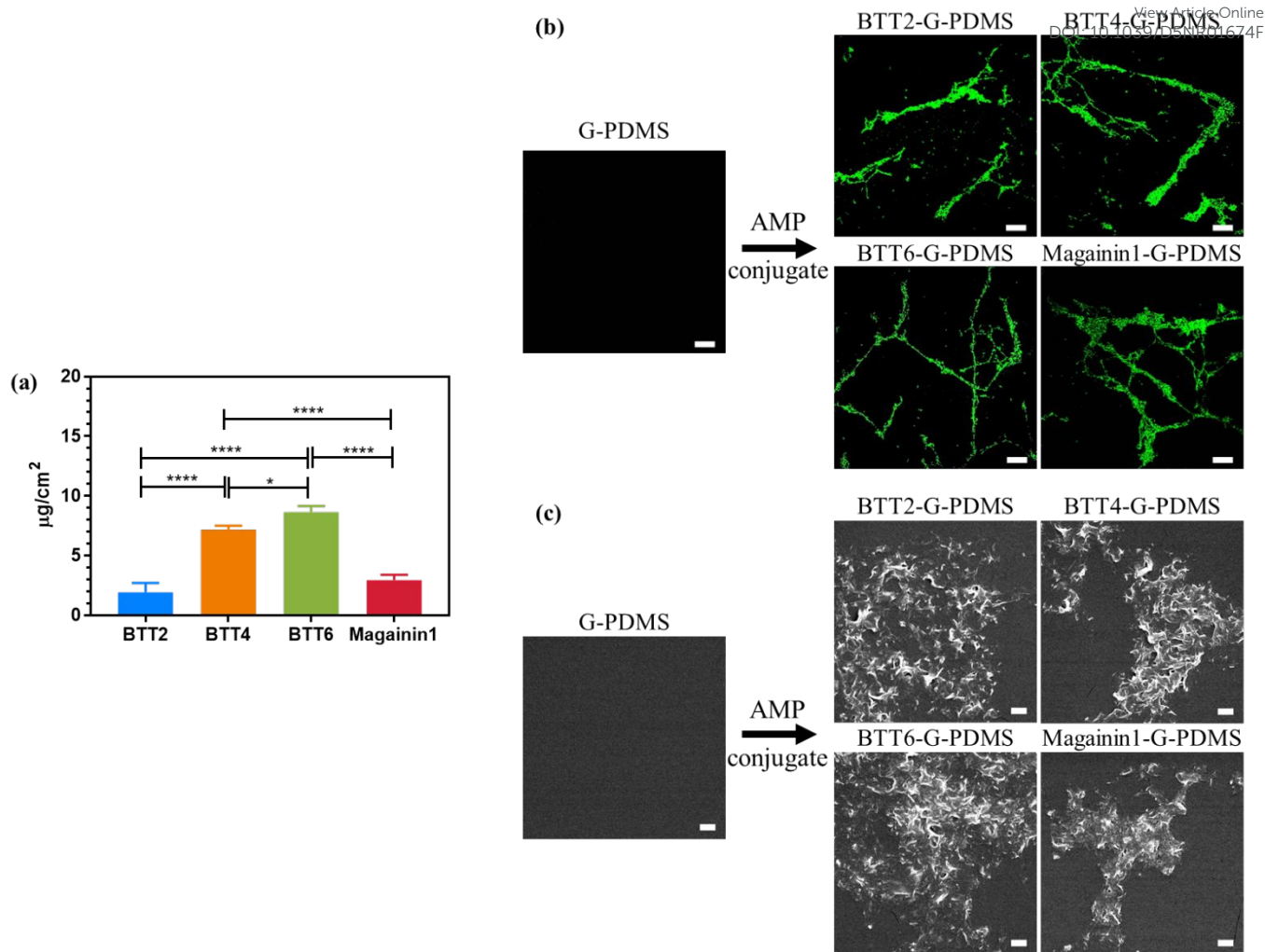


Fig. 5 Characterization of AMP-modified G-PDMS. (a) Quantification of conjugated AMP on G-PDMS. Average amounts of conjugated AMP ($\mu\text{g}/\text{cm}^2$) estimated from calibration curves (Fig. S3). Data are shown as mean \pm SD. Data was analyzed by one-way ANOVA test with post-hoc test (Tukey's multiple comparisons test). Significant differences ($n = 3$, *: $p \leq 0.05$, ****: $p \leq 0.0001$). (b) Distribution of conjugated AMP on G-PDMS. CLSM images of unmodified and AMP-modified graphene coating. Scale bar = 20 μm . (c) Microstructure of AMP-modified G-PDMS. SEM images of unmodified and AMP-modified graphene coating. Scale bar = 1 μm .



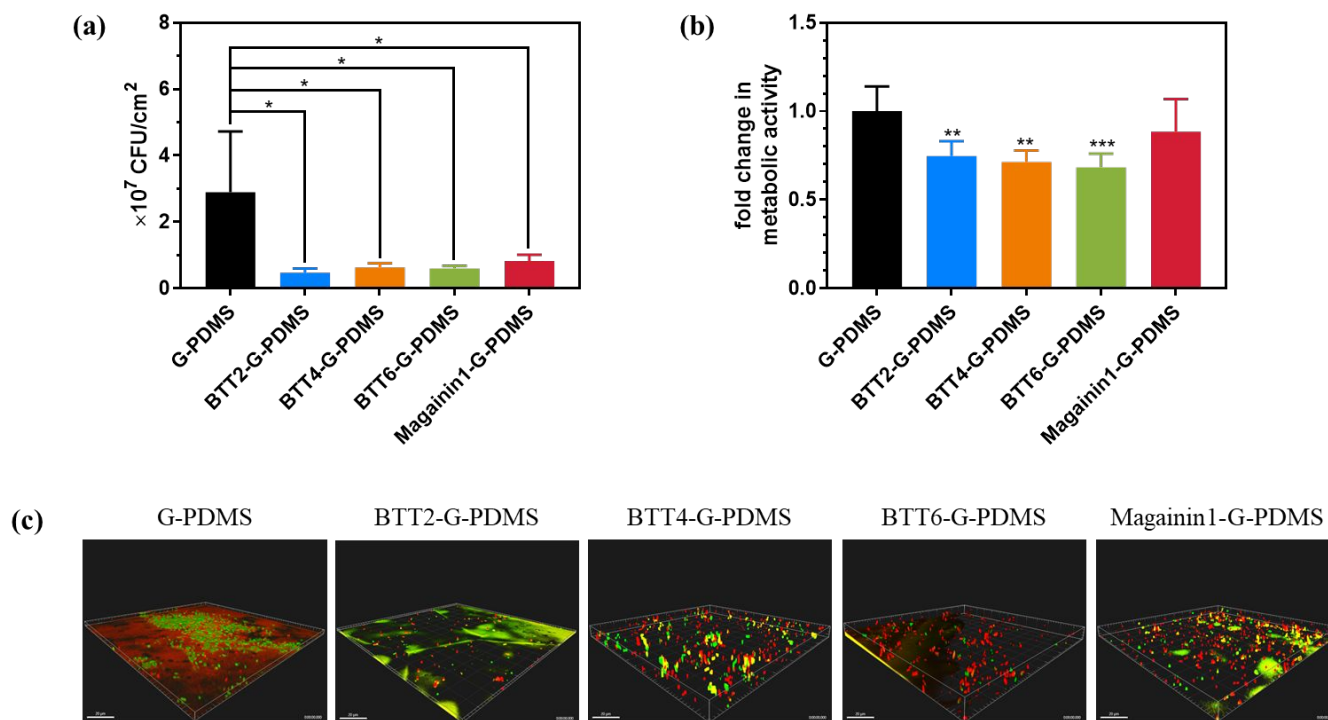


Fig. 6 Effect of AMP-modified CVD graphene coating against *P. aeruginosa*. (a) bacterial adhesion on unmodified and AMP-modified G-PDMS shown in CFU/cm² after 48 h of incubation with *P. aeruginosa*. Data are shown as mean ± SD. Data was analyzed by one-way ANOVA test with post-hoc test (Dunnett's multiple comparisons test). Significant differences ($n = 3$, * $p < 0.05$). (b) microbial metabolic activity of attached bacteria shown in fold change normalized to unmodified surface, in presence of XTT after 4 h of incubation at 37°C ($n = 6$, ** $p < 0.01$, *** $p < 0.001$). (c) 3D confocal images of attached bacteria on unmodified and AMP-modified G-PDMS surface after 48 h of incubation with *P. aeruginosa*. Scale bars = 20 μm.



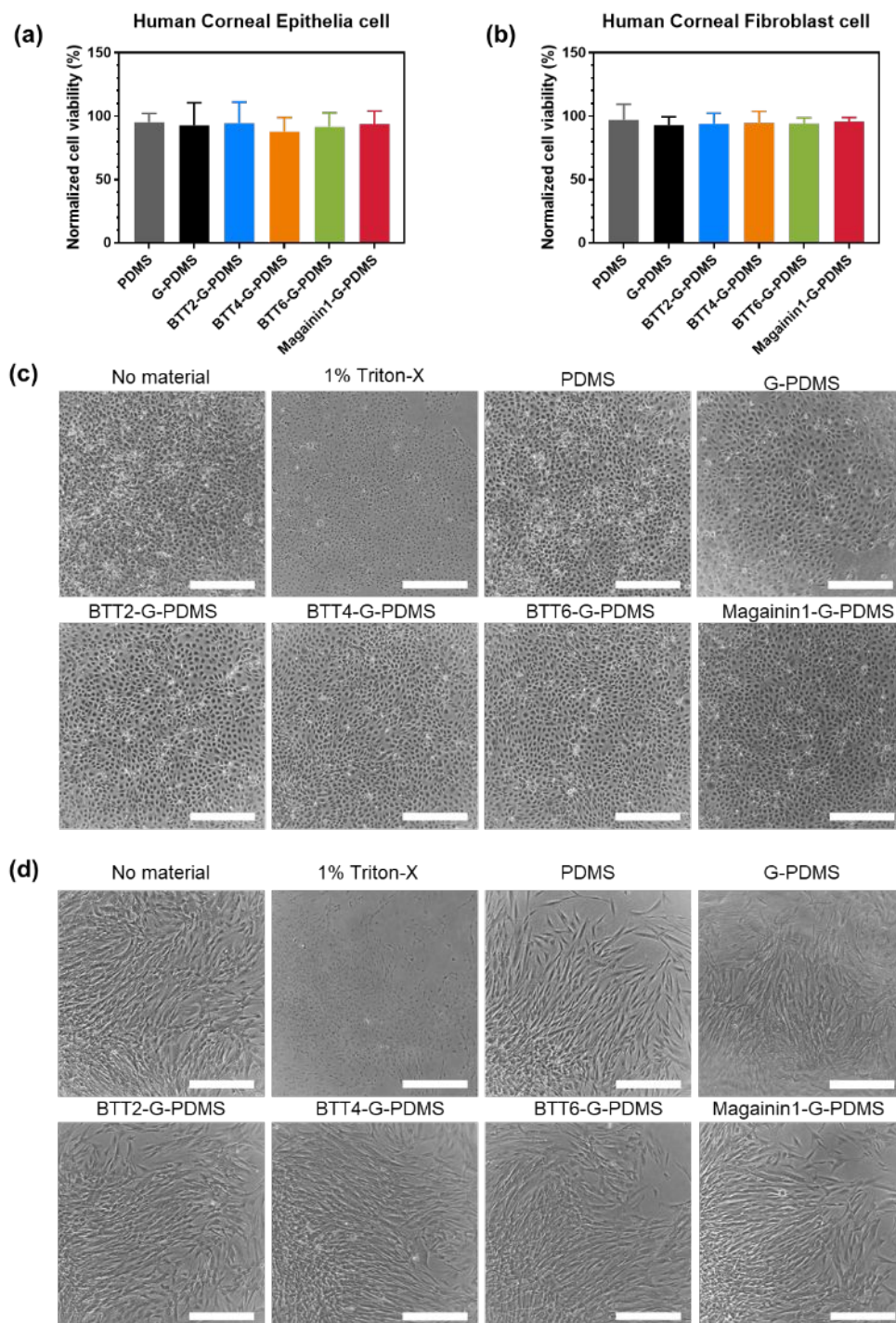


Fig. 7 Cell viability of (a) human corneal epithelia cell and (b) human corneal fibroblast cell after 24 h of incubation with PDMS, unmodified and AMP-modified G-PDMS at 37 °C, 5% CO₂. The viability was measured by the MTS assay and was expressed as a percentage relative to cells grown in the absence of a material. Each treatment condition had two replicates and was repeated three times. Data are shown as mean ± standard deviation. Statistical significance was evaluated using one-way ANOVA ($n = 6$). There was no statistically significant difference between the various treatments ($n = 6$, $p > 0.05$). Representative image of (c) human corneal epithelia cell and (d) human corneal fibroblast cell. Scale bar = 500 µm.



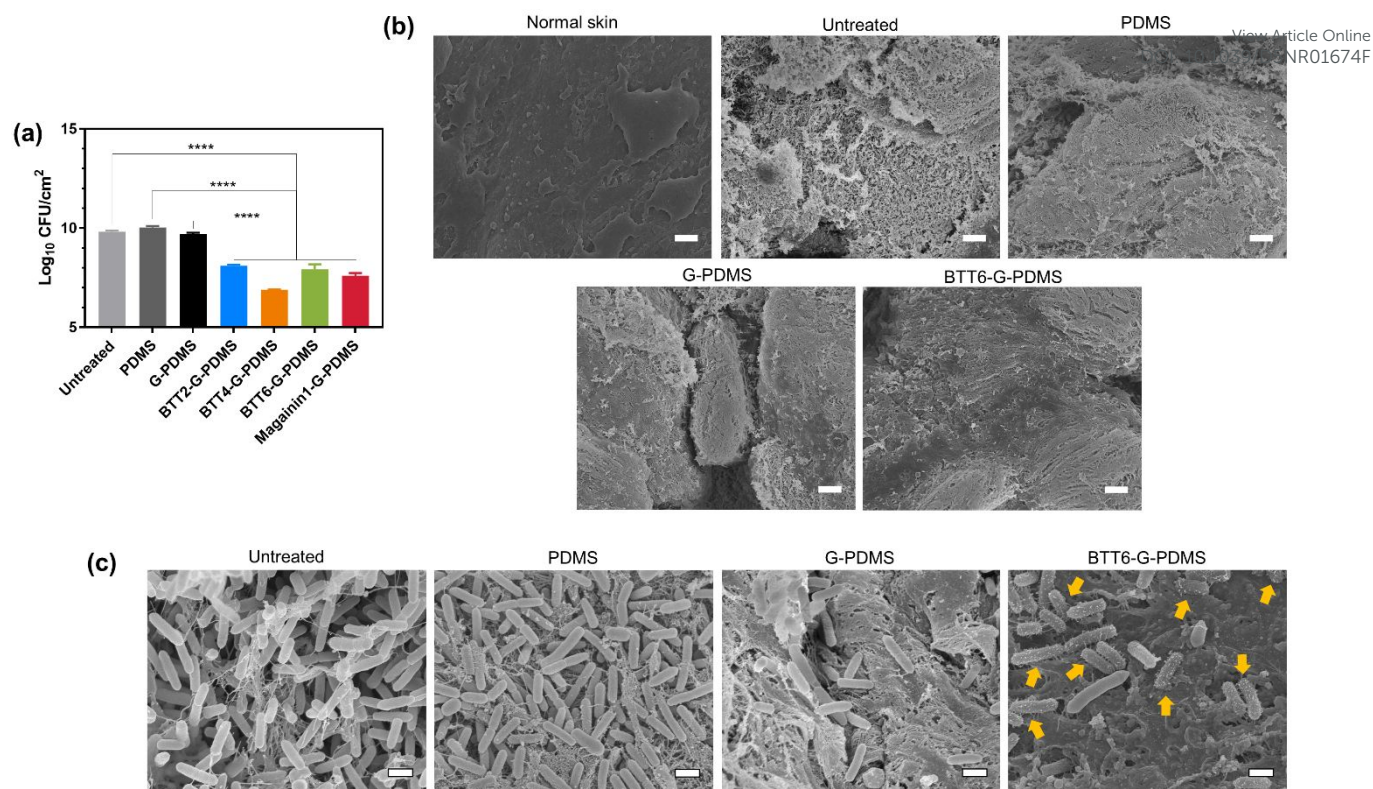


Fig. 8 Bacterial adhesion on skin surface treated by (a) PDMS series shown in CFU/cm^2 after 24 h incubation. ($n = 3$, $**p < 0.01$, $****p < 0.0001$). SEM images of skin surface under magnification (b) 1000 \times (scale bar = 10 μm) and (c) 10,000 \times (scale bar = 1 μm). For each sample, at least three separate positions were viewed.

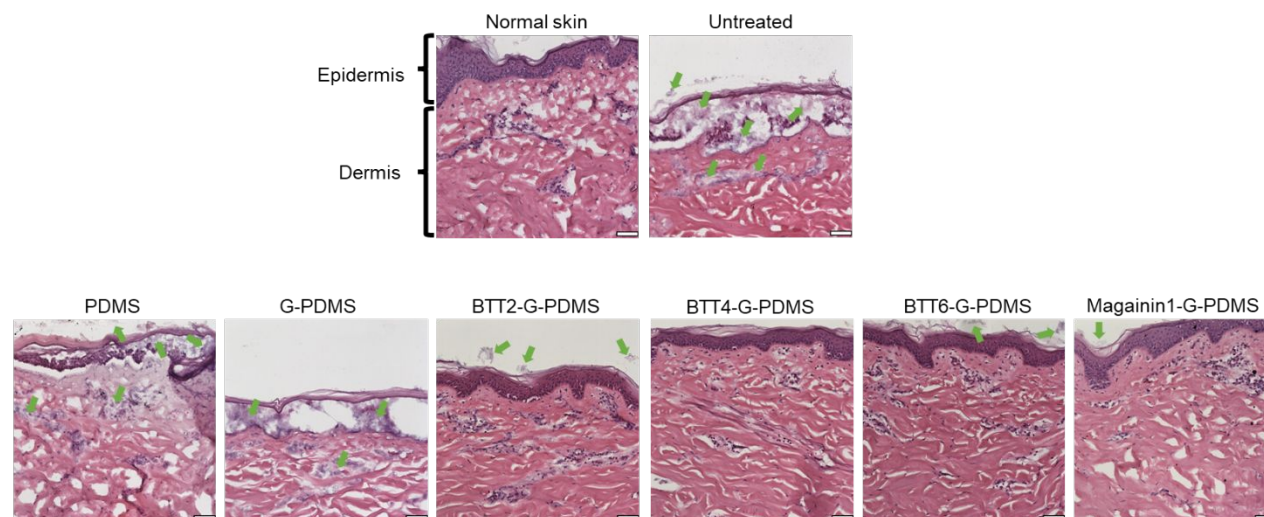


Fig. 9 Hematoxylin and Eosin (H&E) stain of normal skin, infected skin without treatment and infected skin treated with PDMS, G-PDMS, and AMP-modified G-PDMS. Scale bar = 50 μm .



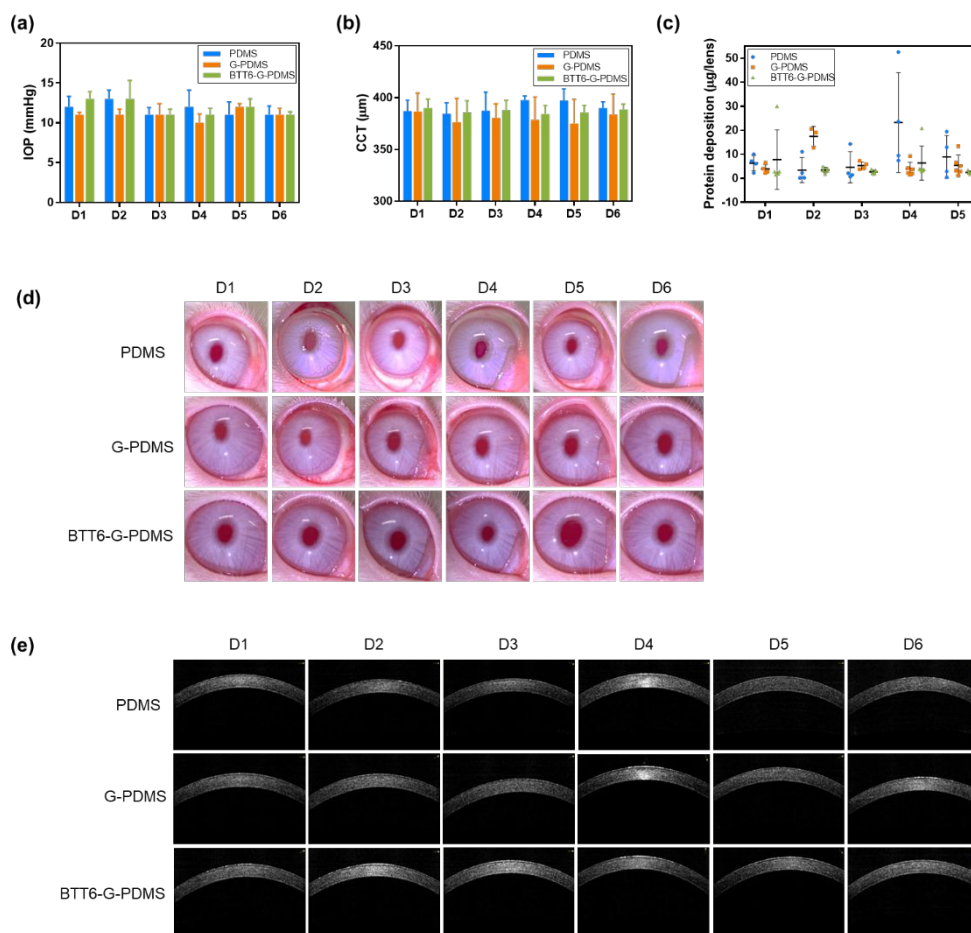


Fig. 10 In vivo biocompatibility of PDMS, G-PDMS and BTT6-G-PDMS as CLs. Daily CLs wearing for up to at least 10 hours per day for 5 days, daily imaging SL, AS-OCT and IOP before lens application, and hourly or more frequent checking of CLs. 3 different CLs material with at least $n=2-3$ animals per group (PDMS $n=4$ eyes, G-PDMS $n=6$ eyes, BTT6-G-PDMS $n=6$ eyes). Male, NZW Rabbit weighing at least 3kg each. (a) IOP Pre and Post CLs application. Normal IOP (10 – 21 mmHg) is maintained throughout 5 continuous changing cycle. (b) CCT measurement by AS-OCT after application of CLs. Statistical significance was evaluated using one-way ANOVA. There was no statistically significant difference between pre and post CLs application ($p > 0.05$). Note that there was no increase in corneal thickness after application of all CLs, confirming excellent biocompatibility. (c) Protein deposition of daily removed CLs. Representative image of (d) SL and (e) AS-OCT. With yellow dry discharge on the eye every morning was observed from G-PDMS group. Absence of any hyper-reflective materials and non-edematous confirm excellent biocompatibility.



The data supporting this article have been included as part of the Supplementary Information. [View Article Online](#)
DOI: 10.1039/D5NR01674F

Open Access Article. Published on 31 July 2025. Downloaded on 8/2/2025 10:31:27 PM.
This article is licensed under a Creative Commons Attribution-NonCommercial 3.0 Unported Licence.

